Energy materials

Synthesis and microwave absorbing properties of γ-Fe₂O₃–SiO₂–poly (3,4-ethylenedioxythiophene) core–shell–shell nanocomposites

Shengning Ji[1,2], Zhiming Zhang[1,2,*] (iD), Xiaohui Jiang[1,2], and Liangmin Yu[1,2,*]

[1] Key Laboratory of Marine Chemistry Theory and Technology, Ministry of Education, Ocean University of China, Qingdao 266100, China

[2] Qingdao Collaborative Innovation Center of Marine Science and Technology, Ocean University of China, Qingdao 266100, China

ABSTRACT

The three-layer core–shell–shell γ-Fe₂O₃–SiO₂–poly (3,4-ethylenedioxythiophene) (PEDOT) nanocomposite has been successfully synthesized by a facile chemical process followed by a detailed investigation of morphology, composition, electromagnetic, and microwave absorption properties. The electrical conductivity of γ-Fe₂O₃–SiO₂–PEDOT nanocomposites was as high as 3.34 S cm^{-1}, and the saturation magnetization was in the range of 1–7 emu g^{-1}. The minimum reflection loss reached -27.5 dB at 13.8 GHz with a matching layer thickness of 2.0 mm and an effective absorption bandwidth (< -10 dB) of about 4.1 GHz (12.0–16.1 GHz). The excellent microwave absorbing performance of this nanocomposite is due to proper impedance matching and the synergistic interaction of dielectric loss, the magnetic loss, and core–shell microstructure. Moreover, the electromagnetic and microwave absorbing properties of γ-Fe₂O₃–SiO₂–PEDOT nanocomposites can be regulated by changing the dosage of functionalized γ-Fe₂O₃–SiO₂.

Introduction

Electromagnetic interference has become a serious problem in recent years, making it urgent to design effective electromagnetic wave absorbers with wide absorption frequency, small reflection loss, and high thermal stability [1–4].

Recently, nanocomposites involving conducting polymers and inorganic nanoparticles have attracted special attention for applications in energy storage, sensors, molecular electronic devices, and electromagnetic interference shielding. For example, polypyrrole with Fe₃O₄ [5], polyaniline with Al₂O₃ [6], TiO₂ [7], and TiC [8] have been prepared by different techniques, and they exhibit synergetic behavior between the polymer and the inorganic material. Especially, magnetic particle and conductive polymer composites form a core–shell structure and have been studied by many groups. Fe₃O₄/PPy [5], Fe₃O₄/PANI [3], and Fe₃O₄/PEDOT [9] core–shell micro- or

Address correspondence to E-mail: zzmcyj@ouc.edu.cn; yuyan@ouc.edu.cn

nanocomposites were prepared and applied in microwave absorption. It has been demonstrated that the core–shell structure has a great advantage in improving the microwave absorption properties due to the interfaces of the core–shell types and its associated interfacial relaxation loss [10–13]. However, it is difficult to ensure that the magnetic particles can be coated uniformly by the conductive polymer, due to the weak interface effect between the magnetic particles and conductive polymers.

Silica is widely used as wave-transmitting material [14, 15]. Moreover, coating silicon on the surface of magnetic particles can shield the magnetic dipolar interaction and favor the dispersion in the solution and thus facilitate the in situ polymerization of a conductive polymer [16]. Due to the superior characters of SiO_2, electromagnetic-functionalized MNPs–SiO_2–CPs core–shell–shell nanocomposites have been designed as wave absorption materials. Among the magnetic metal oxides, Fe_2O_3 has excellent absorptivity due to its high magnetic permeability, saturation magnetization, and good thermal stability. As a typical conductive polymer, poly (3,4-ethylenedioxythiophene) (PEDOT) has been considered as a promising microwave absorbing material because of it being lightweight, easy to synthesize, excellent environmental stability, controllable electrical conductivity, and dielectric loss ability [17, 18]. In this work, γ-Fe_2O_3–SiO_2–PEDOT core–shell–shell nanocomposites were prepared as efficient microwave absorption materials.

According to the absorption mechanism, microwave absorption materials can be classified into two types: magnetic absorbing materials and dielectric absorbing materials [19]. It is well known that only magnetic loss or dielectric loss results in poor electromagnetic impedance matching. Excellent microwave absorption performance can be achieved by combining the magnetic loss and the dielectric loss [20–22]. The efficient complementarity between complex permittivity and permeability and the interfacial effect of core–shell structure in γ-Fe_2O_3–SiO_2–PEDOT nanocomposites are all conducive to improve microwave absorption properties. Furthermore, good electromagnetic impedance matching and the combination of magnetic–dielectric loss can be successfully achieved by regulating the magnetic and electrical properties of γ-Fe_2O_3–SiO_2–PEDOT. Based on a study of the microwave absorption properties of as-prepared composites, we believe that

this type of material will have a brilliant future in microwave absorption.

Experimental

Reagents and materials

$FeCl_3 \cdot 6H_2O$, $FeSO_4 \cdot 7H_2O$, citric acid (CA), tetraethoxysilane (TEOS), and p-toluenesulfonic acid (p-TSA) were purchased from Sinopharm Chemical Reagent Co., Ltd., (Shanghai, China). 3-Mercaptopropyltrimethoxysilane (MPTS) and 3,4-ethylenedioxythiophene (EDOT) were obtained from Aladdin Biochemical Technology Co., Ltd., (Shanghai, China). All reagents were of analytical grade. Distilled water was used in all the experiments.

Synthesis of γ-Fe_2O_3–SiO_2–PEDOT core–shell–shell nanocomposites

The Fe_3O_4 nanoparticles were prepared as reported previously [16]. Briefly, a solution of $FeSO_4 \cdot 7H_2O$ (0.05 mol) and $FeCl_3 \cdot 6H_2O$ (0.1 mol) in 450 mL of deionized water was put in a 500-mL round-bottom flask, then 50 mL of NaOH (6 mol L^{-1}) was slowly dropped into the solution within 2 h under a nitrogen atmosphere. The mixture was reacted at 30 °C and then at 80 °C for 30 min each time. Agitation was undertaken throughout the entire reaction process. Then, precipitates were separated from the solution with a magnet, washed with deionized water and ethanol, and dried in a vacuum at 50 $^+$C for 12 h.

1 g of Fe_3O_4 was pre-treated in citric acid (CA) solution (8.5 g L^{-1}) with ultrasonic processing for 6 h to obtain the functional Fe_3O_4 nanoparticles. These were then dispersed in a mixed solution of water and ethanol (1:4, v:v), and the pH was adjusted using 2.4 mL aqueous ammonia. Next drops of 2 mL of tetraethyl orthosilicate (TEOS) were added with continued ultrasonic vibration for 2 h. The resulting precipitates were separated from the solution with a magnet and heated at 300 °C for 4 h in an air atmosphere. γ-Fe_2O_3–SiO_2 nanoparticles were obtained as described previously [23]. The γ-Fe_2O_3–SiO_2 nanoparticles were functionalized with $-SO_3H$ according to previous literature [24]. γ-Fe_2O_3–SiO_2 nanoparticles (0.5 g) and MPTS (1.0 g) were dispersed in a mixed solution of H_2O_2 and acetic acid with a volume ratio of 1:8. Subsequently, the reaction

was carried out at 80 °C for 2 h with constant mechanical stirring. The resulting precipitates were separated from the solution with a magnet, washed three times with deionized water and with ethanol, and dried in a vacuum at 60 °C for 12 h to obtain γ-Fe_2O_3–SiO_2–SO_3H. Specific amounts of γ-Fe_2O_3–SiO_2–SO_3H nanoparticles and p-TSA were dispersed in distilled water. Next EDOT (0.52 mL, 0.5 mmol) was added to the mixture with ultrasonic vibration for 30 min. Subsequently, $FeCl_3 \cdot 6H_2O$ (20 mmol) solution was slowly added into the above solution. The polymerization was performed at 45 °C for 24 h with constant mechanical stirring. After separating and drying the sediment, γ-Fe_2O_3–SiO_2–PEDOT nanocomposites were obtained.

In this work, γ-Fe_2O_3–SiO_2, γ-Fe_2O_3–SiO_2–SO_3H, and γ-Fe_2O_3–SiO_2–PEDOT were designated as FS, FSS, and FSS_XP, respectively. In FSS_XP, x represents the dosage of FSS.

Characterization

The morphology of the products was investigated using Hitachi S-4800 field emission scanning electron microscope (SEM) and FEI TECNAI G2 F20 transmission electron microscope (TEM). Fourier transform infrared spectrometer (FTIR) was recorded on Bruker Vertex 70 in transmission mode, instrument operated at wave range of 400–2200 cm^{-1} and KBr tableting. The powder X-ray diffraction (XRD) patterns were recorded on a D8 Focus diffractometer (Germany) using Cu-Kα as the radiation in the 2θ range of 5–80 °C. Thermogravimetric analysis (TGA) was carried out on a SETSYS Evolution (Setaram) from 30 to 750 °C under an air atmosphere at a heating rate of 10 °C min^{-1}. Magnetic studies of the samples (saturation magnetization and coercive force) were determined by a vibrating sample magnetometer (VSM, Lakeshore, Model 7404) with an applied voltage of −10 to 10 KOe. The electromagnetic parameters of the samples were investigated using an Agilent E8363B vector network analyzer in the frequency range of 2–18 GHz by the coaxial-line method. The FSS_XP nanocomposites were uniformly mixed with paraffin in a certain mass fraction (30:70wt%), pressing into the ring matrix with the inner diameter of 3.04 mm and outer diameter of 7 mm for measurement.

Results and discussion

The schematic illustration of the process of preparing γ-Fe_2O_3–SiO_2–PEDOT samples is shown in Fig. 1. First of all, Fe_3O_4 was prepared and modified with citric acid to obtain functional Fe_3O_4. Subsequently, Fe_3O_4 was coated with SiO_2 shell through a modified Stöber method [25], and then the obtained Fe_3O_4–SiO_2 was converted to γ-Fe_2O_3–SiO_2 by oxidation. Then, –$(CH_2)_3SO_3H$ was grafted onto a SiO_2 surface through the reaction of MPTS with γ-Fe_2O_3–SiO_2. Finally, the core–shell–shell γ-Fe_2O_3–SiO_2–PEDOT nanocomposites were synthesized by in situ oxidation polymerization of EDOT.

SEM and TEM were taken to characterize the morphology of the FSS_XP nanocomposites. Figure 2a–e shows the morphologies of FSS_XP with different FSS dosages. Apparently, the increase in FSS dosage is beneficial to the homogeneous distribution of γ-Fe_2O_3–SiO_2–PEDOT and to the reduction in γ-Fe_2O_3–SiO_2–PEDOT diameter. Figure 2f shows a typical TEM image of $FSS_{1.0}P$ nanocomposites, which provides sufficient evidence for the existence of a three-layer core–shell–shell structure. The elemental mapping of $FSS_{1.0}P$ further presents the expected core–shell–shell structure clearly in Fig. 3. The images in different colors (Fig. 3c–f) symbolize Fe-, Si-, S-, and C-areas of the $FSS_{1.0}P$, respectively, which confirms that the presence of SiO_2 and PEDOT serves as the shell of the γ-Fe_2O_3 core. It can be seen in Fig. 3h that the C and S elements of PEDOT, Si element of SiO_2, and Fe element of Fe_2O_3 appear at 26, 72, and 106 nm, respectively. It can be calculated that the thickness of the PEDOT shell is 46 nm and the thickness of the SiO_2 shell is about 34 nm. A high-magnification TEM picture (Fig. 3g) and the corresponding EDS line scanning profiles further establish the three-layer core–shell–shell structure of the FSS_XP samples.

The chemical structures of the as-prepared γ-Fe_2O_3–SiO_2–PEDOT nanocomposites were characterized through FTIR spectra, as presented in Fig. 4. The characteristic absorptions at around 568 and 1637 cm^{-1} are attributed to Fe–O linkages of Fe_2O_3. The bending vibration peak and antisymmetric stretching vibration absorption peak of Si–O were present at about 434 and 1090 cm^{-1}, respectively [26]. The other characteristic bands are assigned as follows: The bands observed at 1357 and 1520 cm^{-1} are related to the C–C and C = C stretching vibration of the

Figure 1 A schematic diagram for the fabrication process of as-synthesized γ-Fe$_2$O$_3$–SiO$_2$–PEDOT nanocomposite.
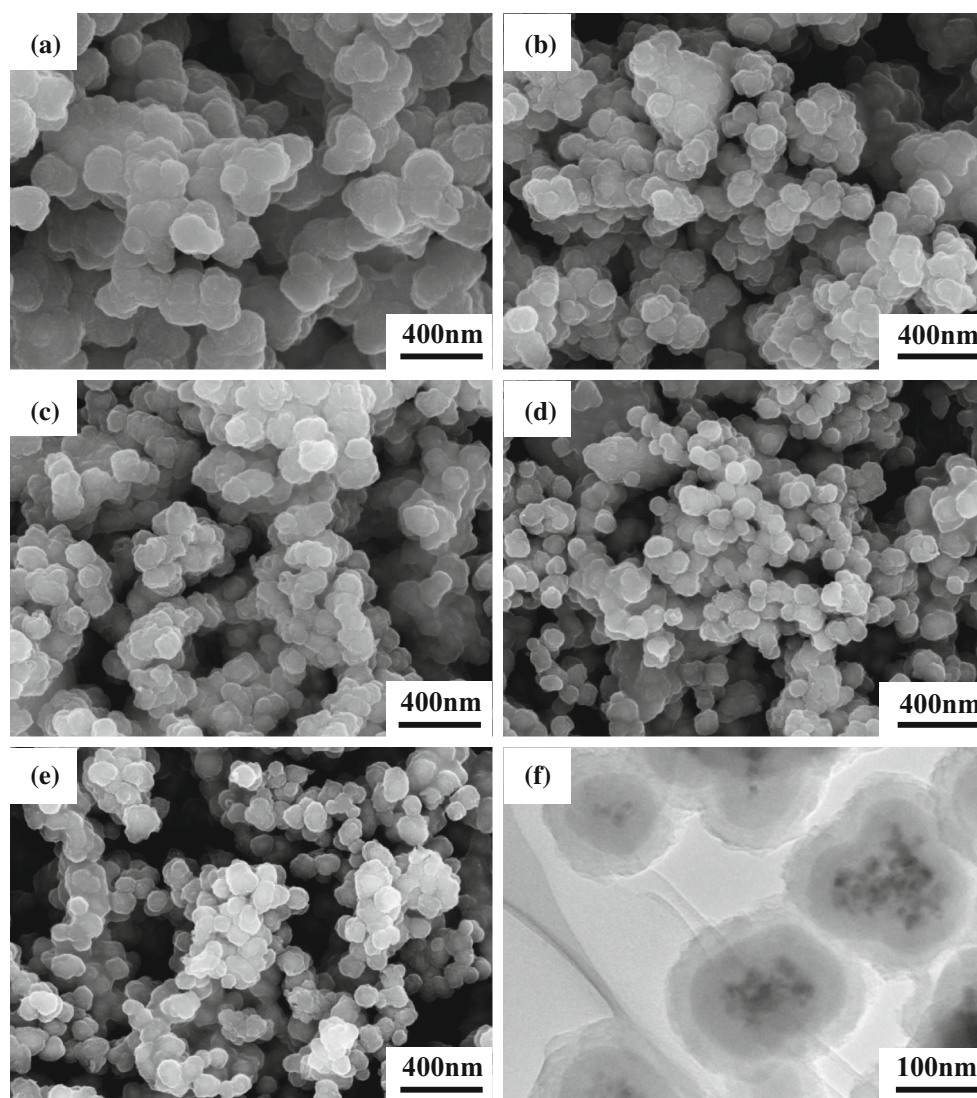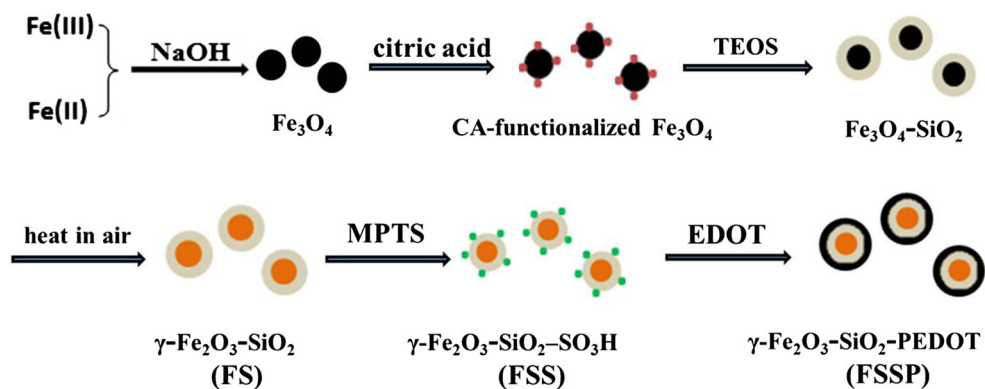
Figure 2 SEM images of **a** FSS$_{0.1}$P, **b** FSS$_{0.3}$P, **c** FSS$_{0.5}$P, **d** FSS$_{0.8}$P, and **e** FSS$_{1.0}$P and TEM image of **f** FSS$_{1.0}$P.

quinoid structure of the thiophene ring, respectively, while C–S–C stretching vibration in the thiophene ring can be seen at 690, 838, 922, and 983 cm^{-1}. The appearance of peaks at 1140 and 1203 cm^{-1} refers to the C–O–C bending vibration of the ethylenedioxy moiety [27, 28]. In a word, the FTIR spectra have given
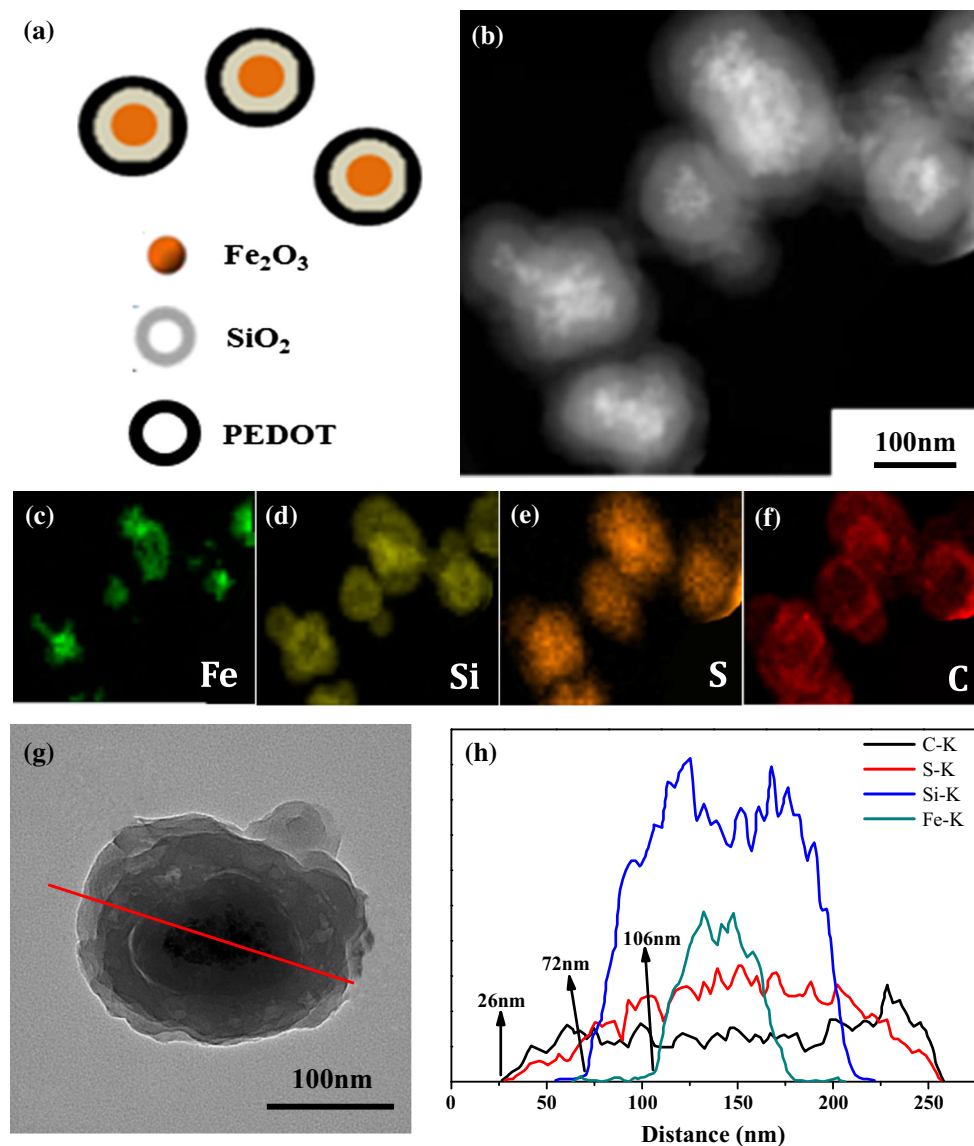
Figure 3 **a** Schematic of γ-Fe₂O₃–SiO₂–PEDOT nanocomposite. **b** HRTEM image of FSS₁.₀P and corresponding elemental mapping images of **c** Fe, **d** Si, **e** S, and **f** C. **g** TEM image of FSS₁.₀P and **h** corresponding EDS line scanning profiles.

further evidence for the successful preparation of γ-Fe₂O₃–SiO₂–PEDOT nanocomposites.

Figure 5 shows the typical XRD patterns of γ-Fe₂O₃–SiO₂–PEDOT nanocomposites. The absorptions at around 30.2°, 35.6°, 43.3°, 53.7°, 57.3°, and 62.9° arise from Fe₂O₃. Apart from the peaks of γ-Fe₂O₃, three main peaks appear at 6.6°, 12.5°, and 26.0° (Fig. 5a–d) corresponding to the PEDOT [29]. However, with the increase in FSS dosage from 0.1 to 1.0 g, the diffraction peaks of PEDOT became weaker, accompanied by the intensity increase in the Fe₂O₃ peaks. It can be seen in Fig. 5e, as the thickness of the PEDOT layer becomes smaller, a diffraction peak

appearing at 23.5 could be readily identified as due to the amorphous SiO₂.

Figure 6 shows the thermogravimetric analysis (TGA) of the samples. It can be clearly seen in Fig. 6b–f that a continuous degradation of FSS$_X$P occurs above 190 °C, and complete decomposition above 450 °C, which is mainly due to the thermal decomposition of PEDOT [30]. Furthermore, it also can be concluded that residual mass fraction of FSS$_X$P increases with the increase in FSS dosage. The content of magnetic FSS cores in the as-prepared FSS$_X$P nanocomposite can be estimated (as shown in Table 1) by the thermogravimetric analysis.
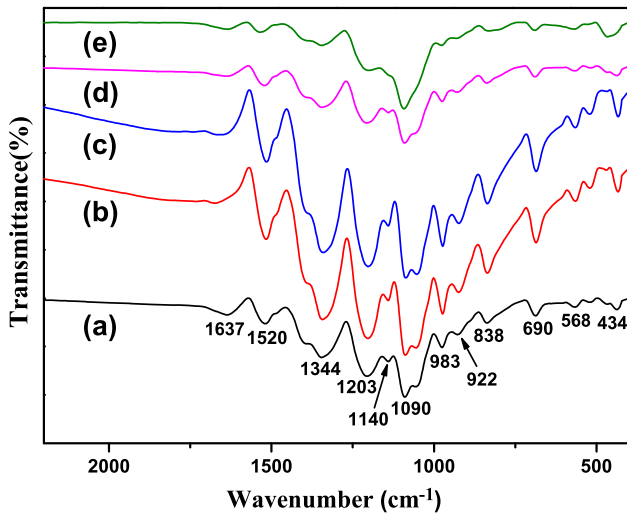
Figure 4 FTIR spectra of (*a*) $FSS_{0.1}P$, (*b*) $FSS_{0.3}P$, (*c*) $FSS_{0.5}P$, (*d*) $FSS_{0.8}P$, and (*e*) $FSS_{1.0}P$.
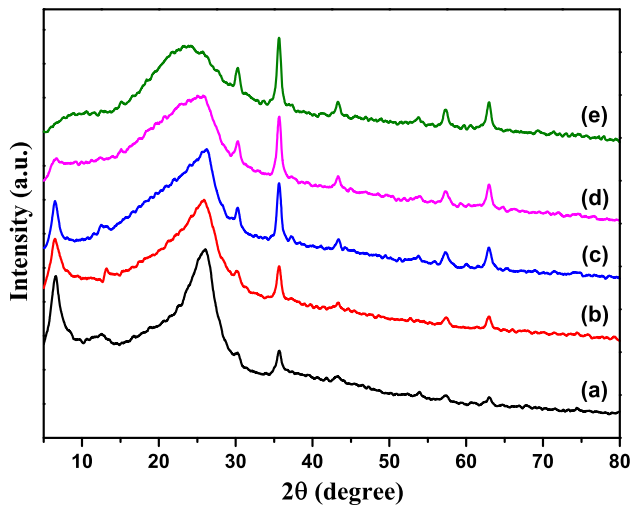
Figure 5 XRD patterns of (*a*) $FSS_{0.1}P$, (*b*) $FSS_{0.3}P$, (*c*) $FSS_{0.5}P$, (*d*) $FSS_{0.8}P$, and (*e*) $FSS_{1.0}P$.

The typical hysteresis loop of as-prepared γ-Fe_2O_3–SiO_2–PEDOT nanocomposites measured at room temperature is presented in Fig. 7. The magnetic parameters corresponding to Fig. 7 are shown in Table 2. With the increase in FSS dosage, the saturation magnetization (M_s) and remnant magnetization (M_r) increased gradually from 1.28 to 6.04 emu g^{-1} and 0.37 to 1.13 emu g^{-1}, respectively, due to the increasing content of FSS in the nanocomposites. Compared with M_s and M_r, the coercivity has changed significantly. It is known that the higher conductivity or lower conductivity is not beneficial to improve microwave absorbing properties [31]. The

electrical properties of FSS_XP are shown in Table 2, and it can be seen that the dosage of FSS has a minor effect on the room temperature conductivity of γ-Fe_2O_3–SiO_2–PEDOT samples, which is in the range of 1 S cm^{-1}. These results indicate that it is possible to regulate the electrical and magnetic properties of γ-Fe_2O_3–SiO_2–PEDOT nanocomposites by changing the content of FSS to realize proper matching between magnetism and electricity, which is confirmed by the wave absorption properties of the γ-Fe_2O_3–SiO_2–PEDOT nanocomposites.

The microwave absorption properties of materials are associated with their complex permittivity and permeability. Generally, the real part (ε') and imaginary part (ε'') of the complex permittivity represent the storage and loss of electric energy, respectively. At the same time, the real part (μ') and imaginary part (μ'') of the permeability symbolize the storage and loss of magnetic energy, respectively [5]. The frequency dependence of the complex permittivity and permeability of the FSS_XP nanocomposite–paraffin is shown in Fig. 8. It can be observed that all electromagnetic parameters (ε', ε'', μ', and μ'') of FSS_XP almost show the same variation in the 2–18 GHz range. As can be seen in Fig. 8a, the values of ε' present a downward tendency in the 2–13 GHz and then show a minor fluctuation in the range of 13–18 GHz. From Fig. 8b, it can be seen that the ε'' values of all samples gradually decrease in the 2–8 GHz and then show an upward trend in the remaining frequency range. This phenomenon is beneficial for the highly efficient complementarity between the permittivity and permeability [32]. The μ' values abruptly decrease and then increase with the frequency increasing in the 2–18 GHz range, as shown in Fig. 8c. It is worth noting that the values of μ'' (Fig. 8d) are positive across the whole range and have apparent peaks at around 7 and 14 GHz, implying the occurrence of natural resonance due to a size effect [33, 34]. It can be speculated that the magnetic loss is mainly caused by the natural resonance of the Fe_2O_3 cores. The above results indicate that the FSS_XP samples present both dielectric loss and magnetic loss.

In general, the excellent microwave absorption properties result from the efficient complementarity between complex permittivity and permeability. The reflection loss (RL) is calculated from the relative permeability and permittivity at the given frequency
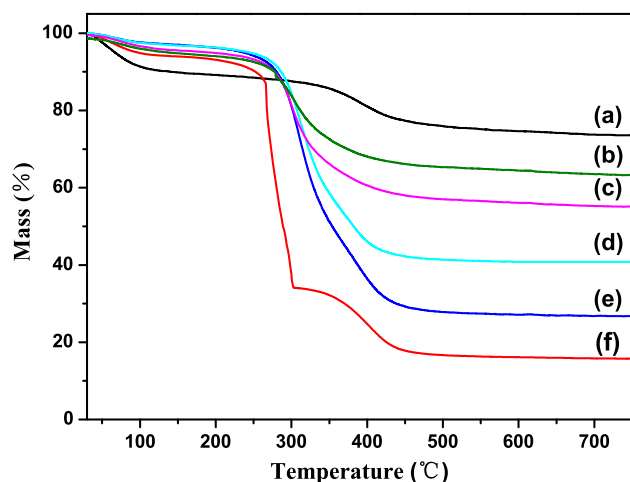
Figure 6 TG curves of (a) FSS, (b) $FSS_{1.0}P$, (c) $FSS_{0.8}P$, (d) $FSS_{0.5}P$, (e) $FSS_{0.3}P$, and (f) $FSS_{0.1}P$.

Figure 7 Hysteresis loops of samples measured at room temperature: (a) FS, (b) $FSS_{1.0}P$, (c) $FSS_{0.8}P$, (d) $FSS_{0.5}P$, (e) $FSS_{0.3}P$, and (f) $FSS_{0.1}P$.
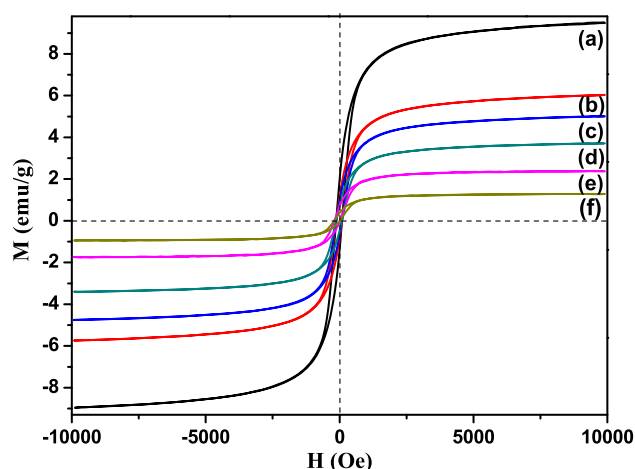
and absorber thickness using the following equations: [35, 36]

$$Z_{in} = \sqrt{\frac{\mu_r}{\varepsilon_r}} \tanh\left[\frac{j2\pi fd\sqrt{\mu_r\varepsilon_r}}{c}\right] \quad (1)$$

$$RL(dB) = 20\log\left|\frac{Z_{in} - 1}{Z_{in} + 1}\right| \quad (2)$$

where Z_{in} is the normalized input impedance of the absorber, μ_r is the relative complex permeability, and ε_r is the complex permittivity. f is the frequency of microwaves, d is the thickness of the absorber, and c is the velocity of light. Additionally, the relative permeability (μ_r) and complex permittivity (ε_r) are expressed as $\mu_r = \mu' - j\mu''$, $\varepsilon_r = \varepsilon' - j\varepsilon''$.

In particular, when the reflection loss (RL) value is less than −10 dB, the material is considered to be effective electromagnetic wave absorber. The typical relationship between the reflection loss and the frequency of samples with different thickness is obtained and shown in Fig. 9. It is clear that the microwave absorbing properties of γ-Fe_2O_3–SiO_2 can be improved greatly by encapsulating within a conductive PEDOT layer. It can be observed that the

reflection loss values of FS (Fig. 9a) are all larger than −10 dB, which indicates the weak microwave absorbing properties. The reflection loss values of FSSxP (Fig. 9b–f) are much lower than that of γ-Fe_2O_3–SiO_2. Especially, $FSS_{0.3}P$, $FSS_{0.5}P$, and $FSS_{0.8}P$ have better microwave absorbing properties. Taking the thickness of 2 mm as an example, the minimum reflection loss of $FSS_{0.3}P$, $FSS_{0.5}P$, and $FSS_{0.8}P$ reaches −27.5 (13.84 GHz), −21.3 (14.19 GHz), and −23.2 dB (17.36 GHz), respectively. The corresponding reflection loss of less than −10 dB is in the wide range of 12.0–16.1, 12.6–16.4, and 13.8–18.0 GHz, respectively. Furthermore, the position of absorbing peak moves to lower frequency with the increase in coating thickness of FSS$_X$P samples.

The study of the normalized input impedance can help to provide a better understanding of the results of reflection loss performance. Impedance matching determines the transmission behaviors of the microwaves. The proper impedance matching can make it possible for the microwave to enter the interior of the materials, which is beneficial to enhance microwave absorption property. As shown in Fig. 10, there are

Table 1 Residual mass of samples in 750 °C and corresponding FSS content

Samples	Residual mass fraction at 750 °C (wt%)	FSS content (wt%)
FSS	73.6	100.0
$FSS_{0.1}P$	15.8	21.5
$FSS_{0.3}P$	26.7	36.3
$FSS_{0.5}P$	40.8	55.4
$FSS_{0.8}P$	55.1	74.9
$FSS_{1.0}P$	62.5	84.9

Table 2 Electrical and magnetic properties of FSS$_X$P nanocomposites

Samples	Conductivity (S cm^{-1})	M_s^a (emu g^{-1})	M_r^b (emu g^{-1})	H_c^c (Oe)
FSS$_{0.1}$P	2.72×10^0	1.28	0.37	8.39
FSS$_{0.3}$P	3.34×10^0	2.37	0.64	20.64
FSS$_{0.5}$P	2.45×10^0	3.71	0.75	62.87
FSS$_{0.8}$P	1.69×10^0	5.01	0.94	76.71
FSS$_{1.0}$P	1.11×10^0	6.04	1.13	93.19

^{a} Saturation magnetization, ^{b} remnant magnetization, ^{c} coercivity
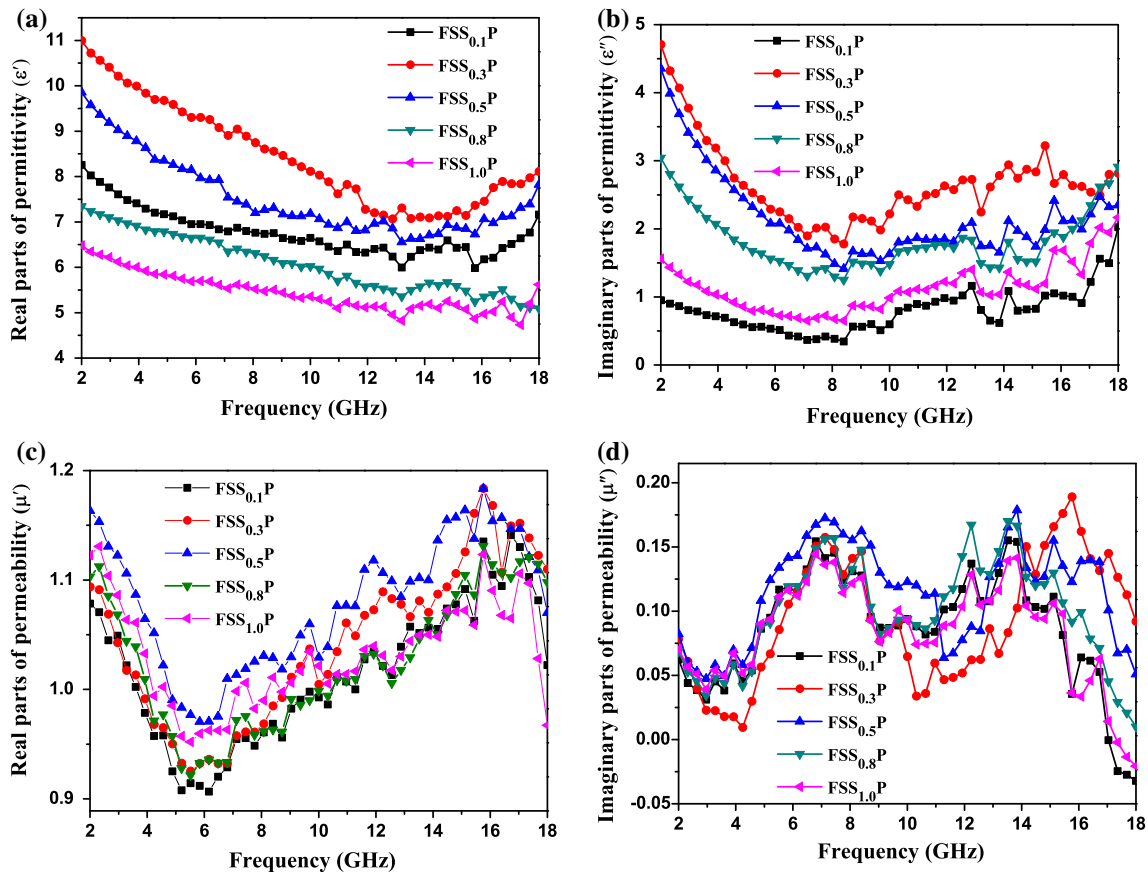
Figure 8 Frequency dependences of **a** real and **b** imaginary parts of complex permittivity and **c** real and **d** imaginary parts of permeability.

no significant differences in the range of 2–14 GHz. From 14.0 to 18 GHz, the input impedance of FSS$_{0.3}$P, FSS$_{0.5}$P, and FSS$_{0.8}$P is much closer to 1 than FSS$_{0.1}$P and FSS$_{1.0}$P. These results correspond to the reflection loss performance, which indicates that the excellent microwave absorption properties of FSS$_X$P can be attributed to its effective impedance matching.

It is well known that the proper layer thickness has a crucial effect on microwave absorption. The electromagnetic wave cancelation effect will occur on the surface of microwave absorbers when the phase difference between the entering wave and the emerging wave is 180° [37]. In this work, the different FSS dosages resulted in different PEDOT layer thickness of FSS$_X$P. That is to say, the proper EM match can be obtained by controlling the dosage of FSS, due to the synergistic interaction of the FSS cores and PEDOT shells, which leads to the excellent microwave absorption properties.

Besides, the special core–shell structure of FSSxP nanocomposites may be advantageous in microwave absorption. In order to confirm this, FSS/PEDOT
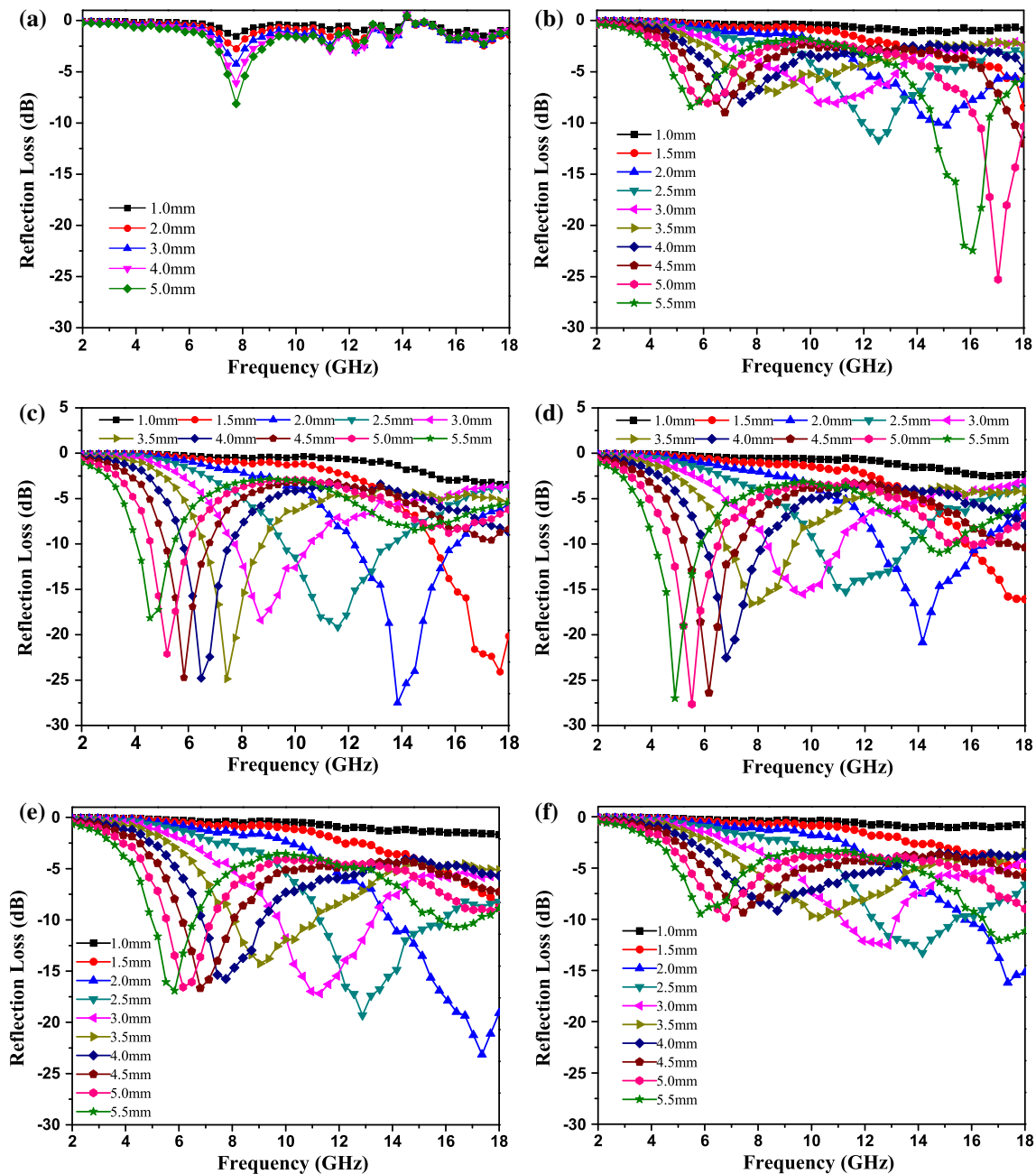
Figure 9 Frequency dependences of reflection loss for samples with different thickness: **a** FS, **b** $FSS_{0.1}P$, **c** $FSS_{0.3}P$, **d** $FSS_{0.5}P$, **e** $FSS_{0.8}P$, and **f** $FSS_{1.0}P$.

composites with the same FSS content as $FSS_{0.3}P$ were prepared by physical blending. The reflection loss properties of core–shell $FSS_{0.3}P$ and physically blended FSS/PEDOT composites are shown in Fig. 11. It was found that the microwave absorption property of $FSS_{0.3}P$ is significantly better than that of blended FSS/PEDOT. This result indicates that interfacial relaxation loss arising from core–shell-type interfaces

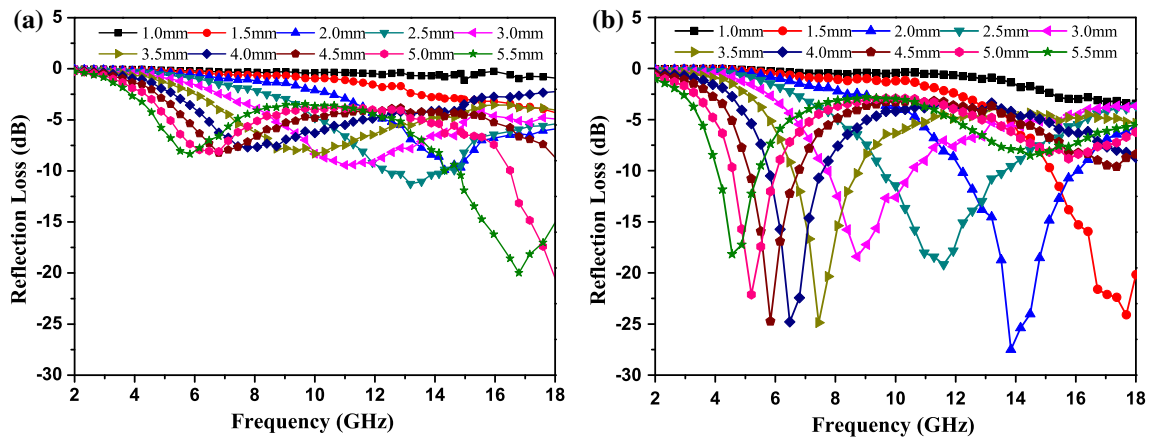between PEDOT and FSS is very beneficial to the microwave absorption properties.

Microwave absorbing performance of various magnetism–CPs composites in previous references is displayed in Table 3. It can be concluded that $FSS_{0.3}P$, $FSS_{0.5}P$, and $FSS_{0.8}P$ have better microwave absorption performance and have more potential to be applied in wide fields.
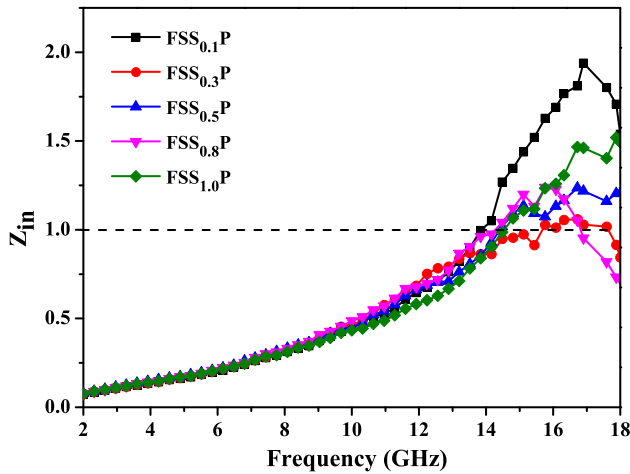
Figure 10 Normalized input impedance of samples with an absorber thickness of 2 mm in the frequency range of 2–18 GHz.

Conclusion

To sum up, γ-Fe$_2$O$_3$–SiO$_2$–PEDOT three-layer core–shell–shell structure nanocomposites have been successfully synthesized by a facile chemical process. The as-prepared samples exhibit ferromagnetic characteristics at room temperature, and the saturation magnetization is in the range of 1–7 emu g^{-1}. The conductivity of γ-Fe$_2$O$_3$–SiO$_2$–PEDOT nanocomposites can reach the magnitude of 3.34 S cm^{-1}. And the lowest reflection loss is -27.5 dB at 13.84 GHz, and corresponding reflection frequency range under -10 dB is 4.1 GHz. The excellent microwave absorption properties mainly attributed to the proper impedance matching in the synergistic interaction of dielectric loss, the magnetic loss, and core–shell microstructure.

Figure 11 Frequency dependences of reflection loss for samples with different thickness: **a** physically blended FSS/PEDOT and **b** FSS$_{0.3}$P.

Table 3 Microwave absorbing performance of various magnetism–CPs composites in previous references

Absorbers	Thickness (mm)	Max RL (frequency)	Effective bandwidth (GHz, RL < −10 dB)	Refs
FexOy@SiO$_2$	2.5	−23.0 dB (9.2 GHz)	3.4	[26]
Fe$_3$O$_4$/MWCNT/PANI	2.0	−8.0 dB (14.7 GHz)	0	[38]
Graphite/CoFe$_2$O$_4$/PANI	2.0	−11.0 dB (3.8 GHz)	0.6	[39]
Fe$_3$O$_4$/PANI	2.0	−13.8 dB (16.7 GHz)	0.9	[40]
Fe$_3$O$_4$/CIP/PANI	2.0	−25.5 dB (10.1 GHz)	2.8	[41]
Graphene@Fe$_3$O$_4$@SiO$_2$@PANI	2.0	−19.4 dB (16.4 GHz)	4.4	[42]
FSS$_{0.3}$P	2.0	−27.5 dB (13.8 GHz)	4.1	This work
FSS$_{0.5}$P	2.0	−21.3 dB (14.1 GHz)	3.8	This work
FSS$_{0.8}$P	2.0	−23.2 dB (17.3 GHz)	4.2	This work

References

[1] Melvin GJH, Ni QQ, Suzuki Y et al (2014) Microwave-absorbing properties of silver nanoparticle/carbon nanotube hybrid nanocomposites. J Mater Sci 49(14):5199–5207

[2] He Q, Yuan T, Zhang X et al (2014) Electromagnetic field absorbing polypropylene nanocomposites with tuned permittivity and permeability by nanoiron and carbon nanotubes. J Phys Chem C 118(42):24784–24796

[3] Sun H, Che R, You X et al (2014) Cross-stacking aligned carbon-nanotube films to tune microwave absorption frequencies and increase absorption intensities. Adv Mater 26(48):8120–8125

[4] Zhao T, Hou C, Zhang H et al (2014) Electromagnetic wave absorbing properties of amorphous carbon nanotubes. Sci Rep 4:5619–5625

[5] Li Y, Chen G, Li Q et al (2011) Facile synthesis, magnetic and microwave absorption properties of Fe_3O_4/polypyrrole core/shell nanocomposite. J Alloy Compd 509(10):4104–4107

[6] Benykhlef S, Bekhoukh A, Berenguer R et al (2016) PANI-derived polymer/Al_2O_3 nanocomposites: synthesis, characterization, and electrochemical studies. Colloid Polym Sci 294(12):1877–1885

[7] Chouli F, Radja I, Morallon E et al (2015) A novel conducting nanocomposite obtained by p anisidine and aniline with titanium (IV) oxide nanoparticles: synthesis, characterization, and electrochemical properties. Polym Compos. doi:10.1002/pc.23837

[8] Radja I, Djelad H, Morallon E (2015) Characterization and electrochemical properties of conducting nanocomposites synthesized from p-anisidine and aniline with titanium carbide by chemical oxidative method. Synth Met 202:25–32

[9] Zhou W, Hu X, Bai X et al (2011) Synthesis and electromagnetic, microwave absorbing properties of core–shell Fe_3O_4–poly (3,4-ethylenedioxythiophene) microspheres. ACS Appl Mater Interfaces 3(10):3839–3845

[10] Dong XL, Zhang XF, Huang H et al (2008) Enhanced microwave absorption in Ni/polyaniline nanocomposites by dual dielectric relaxations. Appl Phys Lett 013127(1):92–94

[11] Liu J, Che R, Chen H et al (2012) Microwave absorption enhancement of multifunctional composite microspheres with spinel Fe_3O_4 cores and anatase TiO_2 shells. Small 8(8):1214–1221

[12] Chen YJ, Zhang F, Zhao G et al (2010) Synthesis, multi-nonlinear dielectric resonance, and excellent electromagnetic absorption characteristics of Fe_3O_4/ZnO core/shell nanorods. J Phys Chem C 114(20):9239–9244

[13] Wang G, Chang Y, Wang L et al (2012) Synthesis, characterization and microwave absorption properties of Fe_3O_4/Co core/shell-type nanoparticles. Adv Powder Technol 23(6):861–865

[14] Qiu J, Wang Y, Gu M (2007) Microwave absorption properties of substituted $BaFe_{12}O_{19}$/TiO_2 nanocomposite multilayer film. J Mater Sci 42(1):166–169

[15] Zhu J, Wei S, Haldolaarachchige N et al (2011) Electromagnetic field shielding polyurethane nanocomposites reinforced with core–shell Fe–silica nanoparticles. J Phys Chem C 115(31):15304–15310

[16] Deng YH, Wang CC, Hu JH et al (2005) Investigation of formation of silica-coated magnetite nanoparticles via sol–gel approach. Colloids Surf A 262(1):87–93

[17] Ohlan A, Singh K, Chandra A et al (2010) Microwave absorption behavior of core–shell structured poly (3,4-ethylenedioxythiophene)–barium ferrite nanocomposites. ACS Appl Mater Interfaces 2(3):927–933

[18] Huo J, Wang L, Yu H (2009) Polymeric nanocomposites for electromagnetic wave absorption. J Mater Sci 44(15):3917–3927

[19] Liu Q, Zhang D, Fan T (2008) Electromagnetic wave absorption properties of porous carbon/Co nanocomposites. Appl Phys Lett 013110(1):93–96

[20] Zhang B, Du Y, Zhang P et al (2013) Microwave absorption enhancement of Fe_3O_4/polyaniline core/shell hybrid microspheres with controlled shell thickness. J Appl Polym Sci 130(3):1909–1916

[21] Belaabed B, Wojkiewicz JL, Lamouri S et al (2012) Synthesis and characterization of hybrid conducting composites based on polyaniline/magnetite fillers with improved microwave absorption properties. J Alloy Compd 527:137–144

[22] Wang G, Gao Z, Tang S et al (2012) Microwave absorption properties of carbon nanocoils coated with highly controlled magnetic materials by atomic layer deposition. ACS Nano 6(12):11009–11017

[23] Zhang Y, Zhang Z, Xu S et al (2016) Synthesis of γ-Fe_2O_3@SiO_2@polypyrrole core/shell/shell nanospheres with flexible controllability of electromagnetic properties. RSC Adv 6(8):6623–6630

[24] Dai T, Yang X, Lu Y (2007) Conductive composites of polypyrrole and sulfonic-functionalized silica spheres. Mater Lett 61(14):3142–3145

[25] Stöber W, Fink A, Bohn E (1968) Controlled growth of monodisperse silica spheres in the micron size range. J Colloid Interface Sci 26(1):62–69

[26] Li HY, Chang CM, Hsu KY et al (2012) Poly (lactide)-functionalized and Fe_3O_4 nanoparticle-decorated multiwalled

carbon nanotubes for preparation of electrically-conductive and magnetic poly (lactide) films and electrospun nanofibers. J Mater Chem 22(11):4855–4860

[27] Zhou H, Yao W, Li G et al (2013) Graphene/poly (3,4-ethylenedioxythiophene) hydrogel with excellent mechanical performance and high conductivity. Carbon 59:495–502

[28] Kvarnström C, Neugebauer H, Blomquist S et al (1999) In situ FTIR spectroelectrochemical characterization of poly (3,4-ethylenedioxythiophene) films. Synth Met 101(1–3):66. doi:10.1016/S0379-6779(98)01133-3

[29] Yin Y, Li Z, Jin J et al (2013) Facile synthesis of poly (3,4-ethylenedioxythiophene) by acid-assisted polycondensation of 5-bromo-2, 3-dihydro-thieno [3,4-b][1,4] dioxine. Synth Met 175:97–102

[30] Gu J, Gao S, Xue Y et al (2016) Synthesis and characterization of PEDOT aqueous dispersions with sulfonated polyfluorene as a template and doping agent. React Funct Polym 100:83–88

[31] Unsworth J, Kaynak A, Lunn BA et al (1993) Microwave transmission, reflection and dielectric properties of conducting and semiconducting polypyrrole films and powders. J Mater Sci 28(12):3307–3312

[32] Liu X, Geng D, Shang P et al (2008) Fluorescence and microwave-absorption properties of multi-functional ZnO-coated α-Fe solid-solution nanocapsules. J Phys D Appl Phys 41(17):5006–5014

[33] Zhang A, Tang M, Cao X et al (2014) The effect of polyethylenimine on the microwave absorbing properties of a hybrid microwave absorber of Fe_3O_4/MWNTs. J Mater Sci 49(13):4629–4635

[34] Zhang XF, Dong XL, Huang H et al (2007) Microstructure and microwave absorption properties of carbon-coated iron nanocapsules. J Phys D Appl Phys 40(17):5383–5387

[35] Naito Y, Suetake K (1971) Application of ferrite to electromagnetic wave absorber and its characteristics. IEEE Trans Microw Theory Tech 19(1):65–72

[36] Zhang D, Cheng J, Yang X et al (2014) Electromagnetic and microwave absorbing properties of magnetite nanoparticles decorated carbon nanotubes/polyaniline multiphase heterostructures. J Mater Sci 49(20):7221–7230

[37] Qiao M, Lei X, Ma Y et al (2016) Well-defined core–shell Fe3O4@Polypyrrole composite microspheres with tunable shell thickness: synthesis and their superior microwave absorption performance in the Ku band. Ind Eng Chem Res 55(22):6263–6275

[38] Cao MS, Yang J, Song WL et al (2012) Ferroferric oxide/multiwalled carbon nanotube vs polyaniline/ferroferric oxide/multiwalled carbon nanotube multiheterostructures for highly effective microwave absorption. ACS Appl Mater Interfaces 4(12):6949–6956

[39] Chen K, Xiang C, Li L, Qian H, Xiao Q, Xu F (2012) A novel ternary composite: fabrication, performance and application of expanded graphite/polyaniline/$CoFe_2O_4$ ferrite. J Mater Chem 22(13):6449–6455

[40] Sun Y, Xiao F, Liu X, Feng C, Jin C (2013) Preparation and electromagnetic wave absorption properties of core–shell structured Fe_3O_4–Polyaniline nanoparticles. RSC Adv 3:22554–22559

[41] He Z, Fang Y, Wang X et al (2011) Microwave absorption properties of PANI/CIP/Fe_3O_4 composites. Synth Met 161(5):420–425

[42] Wang L, Zhu J, Yang H et al (2015) Fabrication of hierarchical graphene@Fe_3O_4@SiO_2@ polyaniline quaternary composite and its improved electrochemical performance. J Alloy Compd 634:232–238